

WHAT LURKS IN THE MARTIAN ROCKS AND SOIL? INVESTIGATIONS OF SULFATES, PHOSPHATES, AND PERCHLORATES

Natural Fe-bearing oxides and sulfates from the Rio Tinto Mars analog site: Critical assessment of VNIR reflectance spectroscopy, laser Raman spectroscopy, and XRD as mineral identification tools†

PABLO SOBRO<sup>1,2,\*</sup>, JANICE L. BISHOP<sup>1,3</sup>, DAVID F. BLAKE<sup>3</sup>, BIN CHEN<sup>3</sup> AND FERNANDO RULL<sup>4</sup>

<sup>1</sup>SETI Institute, 189 Bernardo Avenue, Mountain View, California 94043, U.S.A.

<sup>2</sup>MalaUva Labs, 822 Allen Avenue, St. Louis, Missouri 63104, U.S.A.

<sup>3</sup>NASA Ames Research Center, Moffett Field, California 94035, U.S.A.

<sup>4</sup>Unidad Asociada UVA-Centro de Astrobiología, Edificio INDITI, Av.Francisco Valles 8, Parque Tecnológico de Boecillo, Parcela 203, Boecillo 47151, Spain

ABSTRACT

We have characterized complex iron- and sulfate-bearing samples from Rio Tinto (Spain) using X-ray diffraction (XRD), visible-near infrared reflectance (VNIR) spectroscopy, and laser Raman spectroscopy (LRS). Samples were collected for this study from the Peña de Hierro region of Rio Tinto because this site represents a natural acidic environment that is a potential analog for such environments on Mars. We report an evaluation of the capabilities of these three techniques in performing detailed mineralogical characterization of potential Mars-like samples from a natural acidic terrestrial environment. Sulfate minerals found in these samples include gypsum, jarosite, and copiapite, and iron hydroxide bearing minerals found include goethite and ferrihydrite. These sulfate and iron hydroxide/oxyhydroxide minerals were detected by XRD, VNIR, and LRS. Minor quartz was identified in some samples by XRD as well, but was not identified using VNIR spectroscopy. Coordinating the results from these three techniques provides a complete picture of the mineralogical composition of the samples. Field instruments were used for this study to mimic the kinds of analyses that could be performed in the field or on martian rovers.

**Keywords:** Raman, VNIR reflectance, XRD, sulfates, iron, Mars, analog, Rio Tinto

INTRODUCTION

The surface of Mars contains abundant occurrences of aqueous environments that host sulfates and iron oxide/hydroxide-bearing minerals. The detection of crystalline hematite by the Mars global surveyor thermal emission spectrometer (MGS-TES) (Christensen et al. 2000, 2001) was a main driver for the selection of Meridiani Planum as the landing site for the NASA's Mars Exploration Rover (MER) Opportunity. TES studies contributed to the understanding of the occurrence of hematite; geochemical considerations led to the conclusion that the most plausible mechanism for the occurrence of the hematite units was precipitation from Fe-rich water.

Identification of hydrous sulfates in several bright regions including Paso Robles and Tyrone at Gusev crater (Gellert et al. 2006; Haskin et al. 2005; Johnson et al. 2007; Lane et al. 2008; Ming et al. 2008; Parente et al. 2009; Wang et al. 2008, 2006) and the alleged findings of jarosite in the Meridiani regolith (Klingelhofer et al. 2004), at Mawrth Vallis (Farrand et al. 2009), and at Noctis Labyrinthus (Weitz et al. 2011) provide evidence for former aqueous processes on Mars.

Massive accumulations of sulfates have also been detected

remotely using data from the OMEGA (Observatoire pour la Minéralogie, l'Eau, les Glaces, et l'Activité) instrument on ESA's Mars Express (Bibring et al. 2007; Gendrin et al. 2005) and the Compact Reconnaissance Imaging Spectrometer for Mars (CRISM) instrument on NASA's Mars Reconnaissance Orbiter (Bishop et al. 2009; Flahaut et al. 2010; Lichtenberg et al. 2010; Murchie et al. 2009; Roach et al. 2009, 2010; Sowe et al. 2012; Wiseman et al. 2010).

Sulfates were also detected at the Phoenix landing site (Smith et al. 2009). More recently, the ChemCam instrument onboard the Mars Science Laboratory rover, Curiosity, has identified the presence of Ca-sulfates at Rocknest (Clegg et al. 2013; Tokar et al. 2013). The presence of the sulfate mineral species listed above not only constitutes evidence regarding the environmental history of a particular region (Meslin et al. 2013), but may define the potential habitability of an environment (Boston et al. 2001).

The Rio Tinto acid mine drainage-dominated region features numerous settings where sulfates and iron oxide/hydroxide species have formed (Amils et al. 2007; Fernández-Remolar et al. 2005, 2011). These studies have shown that both inorganic and biologic activity plays a role in formation of many of the precipitates and efflorescent salts in this region. Given the association of microorganisms such as *Acidithiobacillus ferrooxidans* with the aqueous oxidation of sulfides in Rio Tinto (Amils et al. 2002), deposits of sulfate precipitates on Mars represent possible sites to search for extinct life on that planet.

\* E-mail: psobron@seti.org

† Special collection papers can be found on GSW at <http://ammin.geoscienceworld.org/site/misc/specialissuelist.xhtml>.

Lab and field investigations of iron-rich aqueous precipitates and alteration environments are needed to provide ground-truthing for identification of these minerals on Mars and to improve our ability to connect the martian mineralogy to geochemical environments. For this study, we used three techniques for a mineralogical investigation that are currently employed or planned for landed missions on Mars: X-ray diffraction (XRD), visible-near infrared (VNIR) reflectance spectroscopy, and laser Raman spectroscopy (LRS).

The goals of our investigation are to: (1) characterize the complex iron and sulfate-bearing samples from a site at Rio Tinto (SW Spain); (2) compare measurement type, analysis, and results of these three techniques to perform detailed mineralogical characterization of potential Mars-like samples from a natural acidic terrestrial environment; and (3) provide a collection of diffraction and spectral data that can help interpret mission data.

## METHOD

### Samples

Efflorescences and precipitates associated with acidic surface stream waters were collected from several sites near Peña de Hierro; this is the main source of the natural acid mine drainage characteristic of Rio Tinto. Figure 1 shows a context image of the Peña de Hierro sampling site and images of the four samples analyzed. The samples were collected from the banks of the stream as indicated in the figure and sealed in plastic bags to minimize transformation of the minerals. The pH in our sampling site was  $\sim 3$  at the time samples were collected. The samples were analyzed in the laboratory within two weeks of collection. Although transformation of the samples was possible during storage and transport, we tried to minimize this through careful sample handling. VNIR and LRS measurements were performed on unprepared samples. Sample preparation for XRD was performed prior to measurement. In situ mineralogical analyses of samples from the Rio Tinto site have been reported elsewhere (Sobron et al. 2011).

### X-ray diffraction analyses

Powder X-ray diffraction was performed using inXitu's Terra instrument, a field-portable version of the CheMin instrument aboard NASA's Mars Science Laboratory (MSL) mission (Blake et al. 2012; Sarrazin et al. 2008). Terra utilizes a  $\text{CoK}\alpha$  X-ray tube, and its  $2\theta$  range is  $4\text{--}55^\circ$ . Samples were gently crushed and sieved prior to the analyses to achieve particles about  $150\text{ }\mu\text{m}$  in size. Mineral identification was carried out through peak comparison against the International Centre for Diffraction Data's (ICDD) Powder Diffraction File (PDF) mineral database. Quantitative results were obtained through Rietveld refinement or full pattern fitting techniques (Rietveld 1969).

### Visible-near infrared reflectance spectroscopy analyses

VNIR reflectance spectra were measured using a FieldSpecProFR from Analytical Spectral Devices (ASD) with a contact probe and solar simulated light source. Spectra were measured relative to a halon white reference from spots  $\sim 1\text{ cm}$  across on the rock surfaces at  $2\text{ nm}$  spectral resolution from  $0.35$  to  $2.50\text{ }\mu\text{m}$ . Spectra were collected at several locations on the rock surfaces without preparation. Minerals were identified by comparing the data with spectra of minerals in library collected by co-author Bishop. Reflectance spectra of the natural samples are darker than the lab mineral spectra. This is because the natural samples are all solid coatings on rock surfaces, while the mineral spectra are all particulate samples.

### Laser Raman spectroscopy analyses

The samples were placed on a 3D-motion stage of an inVia Raman microscope (Renishaw), and analyzed using  $20\times$  objective lenses. The  $632.8\text{ nm}$  line from a Renishaw He-Ne laser was used as the excitation source. Laser power at the sample was measured as  $1\text{ mW}$ , and the spot size was  $50\text{ }\mu\text{m}$ . The spectra were recorded within the region  $100\text{--}3700\text{ cm}^{-1}$  with a spectral resolution of  $4\text{ cm}^{-1}$ . Samples were analyzed without preparation. An average of five spots were analyzed on the surface of each of the samples; all of the spectra recorded for each sample were averaged, thus yielding a single spectra per sample that accounts for inhomogeneities in the samples. The LRS spectra were analyzed in three regions

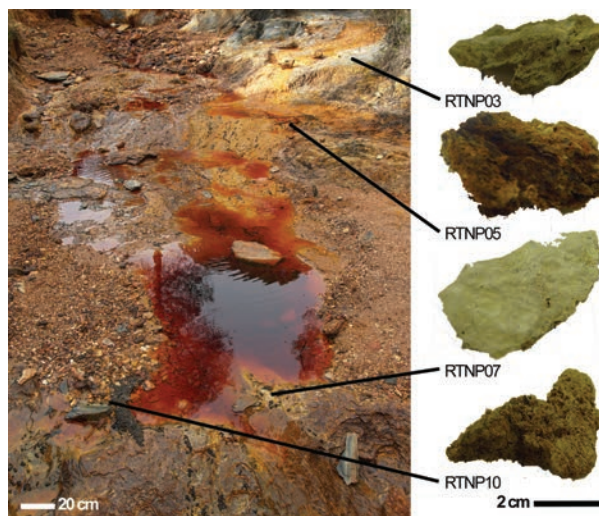


**FIGURE 1.** Pictures of the sampling site, located at  $37^\circ43'18.69''\text{ N}$   $6^\circ33'33.24''\text{ W}$ , and pictures of the samples used for this study. (Color online.)

of interest: low wavenumbers ( $100$  to  $800\text{ cm}^{-1}$ ), mid wavenumbers ( $800$  to  $1300\text{ cm}^{-1}$ ), and high wavenumbers ( $3100$  to  $3700\text{ cm}^{-1}$ ). The spectra were filtered and baseline-corrected using improved fast-Fourier transform algorithms. Routines based on the Marquardt method (Marquardt 1963) were used to analyze the spectra in terms of band position, intensity, width, and Gaussian-Lorentzian (G-L) factor (Sobron et al. 2008). The LRS spectra were interpreted in terms of the fundamental molecular vibrational modes that shape the spectral profiles.

## RESULTS AND DISCUSSION

Figures 2 to 4 show the XRD pattern and the VNIR and LRS spectra of sample RTNP03, respectively. The XRD pattern of this sample is contributed mainly by gypsum,  $\text{CaSO}_4\cdot 2\text{H}_2\text{O}$ . The additional peaks in this pattern are likely due to Na-jarosite,  $\text{NaFe}_3^+(\text{SO}_4)_2(\text{OH})_6$  and quartz,  $\text{SiO}_2$ . The strong water combination bands in the RTNP03 VNIR spectra near  $1.45$  and  $1.95\text{ }\mu\text{m}$  and the small shoulder near  $1.76\text{ }\mu\text{m}$  are highly consistent with gypsum (Bishop et al. 2004). Jarosite contains features at  $0.43$ ,  $0.89$ ,  $1.46$ ,  $1.85$ , and  $2.26\text{ }\mu\text{m}$  (Bishop and Murad 2005) that correspond well to the features observed in the spectra of RTNP03. Goethite exhibits a broader  $\text{Fe}^{3+}$  transition than jarosite and reflectance peaks at  $0.59$  and  $0.76\text{ }\mu\text{m}$  (Bishop et al. 2004) that could be contributing to the RTNP03 spectra as well.

The Raman spectrum of sample RTNP03 corresponds to that of a sulfate rich minerals; it is mainly composed of bands arising from sulfate molecular vibrations and water. In aqueous systems, the  $\nu_1$ ,  $\nu_2$ ,  $\nu_3$ , and  $\nu_4$  degenerate vibrational modes of sulfate give rise to bands at  $982$ ,  $450$ ,  $1105$ , and  $625\text{ cm}^{-1}$ , respectively (Nakamoto 1997). A split of these sulfate vibrational modes into separate bands is observed in the crystal structures (Frost et al. 2005; Sasaki et al. 1998) and is due to symmetry breakdown. This effect is readily observed in the Raman spectra of samples RTNP03, particularly the splitting of the sulfate bands in the  $1000\text{--}1300\text{ cm}^{-1}$  region. The two sets of bands centered around  $450$  and  $600\text{ cm}^{-1}$  in the spectrum of RTNP03 are attributed to the  $\nu_2$  and  $\nu_4$  vibrational modes of the sulfate tetrahedral oxyanions, respectively. The above discussion applies to the Raman spectra of samples RTNP05, 07, and 10 discussed below.

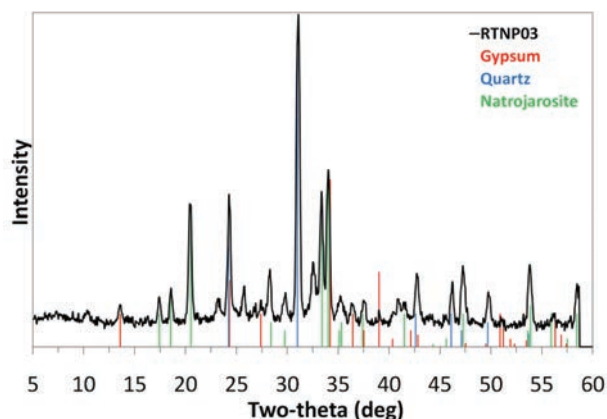


FIGURE 2. XRD pattern of sample RTNP03. The main peaks in the pattern match those of quartz (red), gypsum (blue), and Na-jarosite (green). (Color online.)

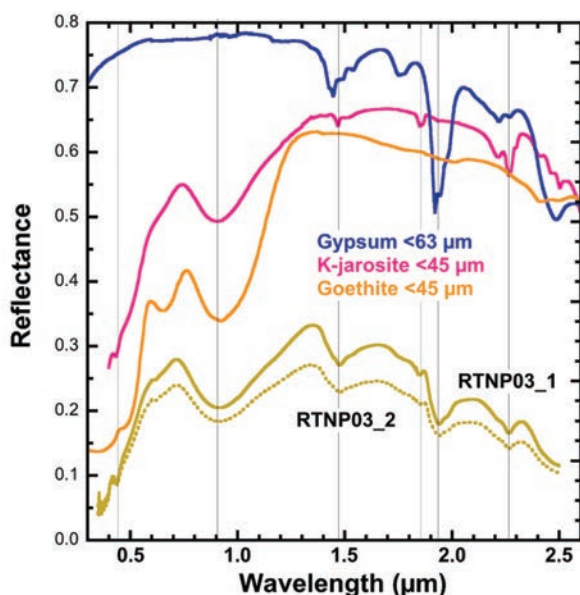
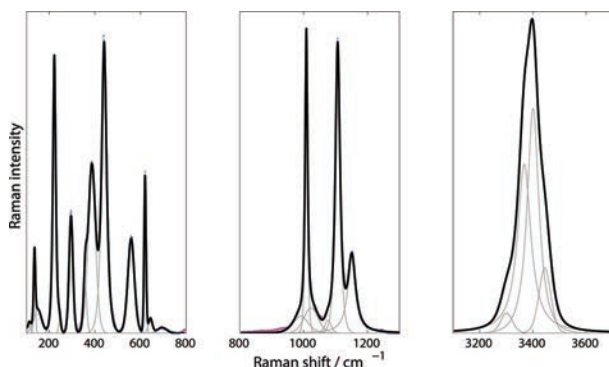


FIGURE 3. VNIR reflectance spectrum of sample RTNP03. The spectra compare to those of gypsum (JB556), jarosite (JB53), and likely goethite (JB54). (Color online.)



The RTNP03 Raman spectrum shows characteristic features of jarosite in the high-wavenumber region: an intense band at  $3401\text{ cm}^{-1}$  with two shoulders at  $3367$  and  $3445\text{ cm}^{-1}$  (Chio et al. 2005; Frost et al. 2006). It is likely that additional bands are contributing to the complex the spectral envelope of sample RTNP03 in the high-wavenumber region, including gypsum. The identification of the latter is, however, not unambiguous. Finally, a strong band is observed at  $386\text{ cm}^{-1}$ , attributed to a vibration of the  $[\text{Fe}(\text{H}_2\text{O})_6]^{2+}$  complex (Hester and Plane 1964; Sobron et al. 2007). Based on our interpretation of the Raman spectrum, we suggest that sample RTNP03 is composed of jarosite, an unidentified hydrated  $\text{Fe}^{2+}$  sulfate, and possibly gypsum.

Figures 5 to 7 show the XRD pattern and the VNIR and LRS spectra of sample RTNP05, respectively. The XRD pattern of this sample is contributed mainly by gypsum, and shows peaks related to goethite,  $\text{FeO}(\text{OH})$ , and ferrihydrite,  $\text{Fe}_2^+\text{O}_3 \cdot 0.5(\text{H}_2\text{O})$ . Two areas of the RTNP05 samples were analyzed with VNIR reflectance. VNIR spectrum RTNP05\_01 is consistent with jarosite, gypsum, and goethite as in the spectra of sample RTNP03. VNIR spectrum RTNP05\_02 lacks the jarosite features and exhibits broader water bands at shorter wavelengths and a broader  $\text{Fe}^{3+}$  band at longer wavelengths more consistent with ferrihydrite (Bishop and Murad 2002) and ferricopiapite (Bishop et al. 2005). The  $\text{Fe}^{3+}$  reflectance peak near  $0.6\text{ }\mu\text{m}$  is also consistent with goethite. However, these are not unique mineral assignments and other Fe-bearing minerals also have features that are similar.

Two Raman spectra, RTNP05a and RTNP05b, were recorded from the RTNP05 sample; the LRS spectra are collocated with the VNIR spectra discussed above. The Raman spectrum RTNP05b shows two intense bands at  $1006$  and  $1137\text{ cm}^{-1}$ . These bands are characteristic of gypsum (Krishnamurthy and Soots 1971). The  $412/491\text{ cm}^{-1}$  and the  $617/668\text{ cm}^{-1}$  doublets originate from the degenerate sulfate  $\nu_2$  and  $\nu_4$  vibrational modes, respectively. Additionally, the pair of bands located in the water-stretching region around  $3405$  and  $3491\text{ cm}^{-1}$  are indicative of the presence of two water molecules in the unit cell, consistent with gypsum.

The Raman spectrum RTNP05a shows a sharp intense band at  $3405\text{ cm}^{-1}$  with two shoulders at  $3371$  and  $3443\text{ cm}^{-1}$ , consistent with jarosite (Chio et al. 2005; Frost et al. 2006). An additional band is observed at  $3497\text{ cm}^{-1}$ , likely related to additional water molecules associated with other cations, e.g., gypsum. Based on the interpretation of the Raman spectra recorded from sample RTNP05, our conclusion is that the RTNP05 sample contains both jarosite and gypsum.

Figures 8 to 10 show the XRD pattern and the VNIR and LRS spectra of sample RTNP07, respectively. The XRD pattern of sample RTNP07 includes contributions from copiapite, jarosite, and quartz. The VNIR reflectance spectra of two spots on the surface of the RTNP07 sample compare well to particulate samples of gypsum (JB556)  $<63\text{ }\mu\text{m}$  and ferricopiapite (JB620)  $<125\text{ }\mu\text{m}$ . The  $\text{Fe}^{3+}$  bands at  $0.43$  and  $0.87\text{ }\mu\text{m}$  are characteristic

◀ FIGURE 4. Raman spectrum (red circles) of sample RTNP03 in three regions of interest, spectral bands (gray), and fitted spectrum (black). Jarosite, gypsum, and a hydrated iron sulfate were identified based on the position and relative intensity of the spectral bands. (Color online.)



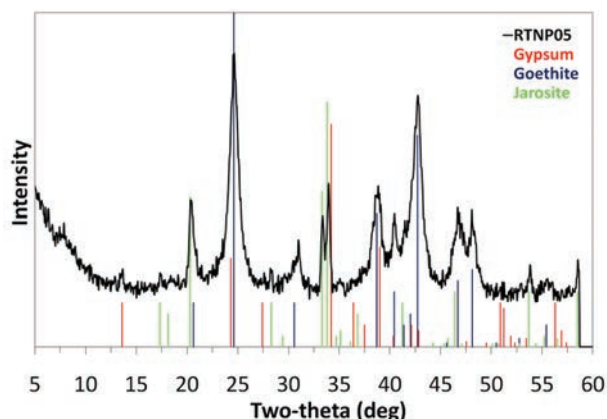


FIGURE 5. XRD pattern of sample RTNP05. The main peaks in the pattern match those of gypsum (green), goethite (blue), and jarosite (red). (Color online.)

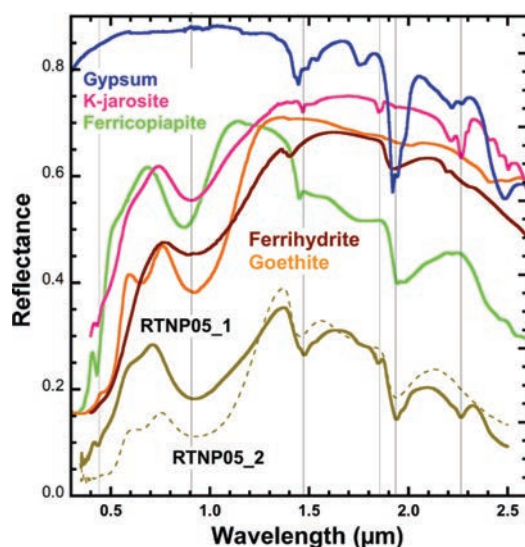
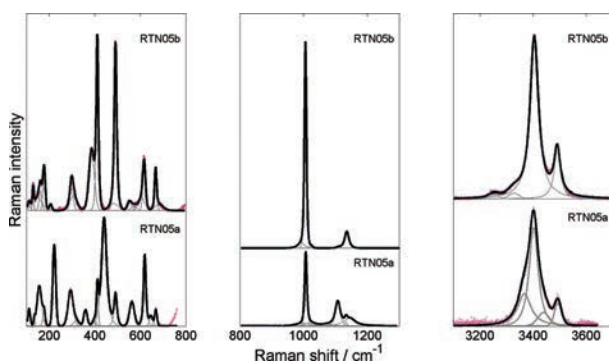


FIGURE 6. VNIR reflectance spectra of sample RTNP05. The spectra compare to those of gypsum (JB556), jarosite (JB53), goethite (JB54), ferrihydrite (JB499), and ferricopiapite (JB620). Unidentified Fe-bearing minerals may be present in the sample. (Color online.)



of ferricopiapite (Bishop et al. 2005). The water bands at 1.44 and 1.93  $\mu\text{m}$  are consistent with a combination of ferricopiapite and gypsum, and the weak feature at 2.2  $\mu\text{m}$  is consistent with gypsum.

The complex envelope around 1000  $\text{cm}^{-1}$  in the Raman spectrum of the RTNP07 sample confirms the presence of multiple cation-sulfate bondings. The sharp band at 3526  $\text{cm}^{-1}$  may be assigned to  $\text{Fe}^{3+}$  or  $\text{Fe}^{2+}$ -OH vibrations, and the broad continuum around 3200  $\text{cm}^{-1}$  may be associated with water stretching vibrations; therefore, the RTNP07 sample contains hydrous  $\text{Fe}^{2+}$  and  $\text{Fe}^{3+}$  oxides, likely belonging to the copiapite group, as suggested by the XRD and VNIR reflectance analyses.

Figures 11 to 13 show the XRD pattern and the VNIR and LRS spectra of sample RTNP10. The XRD pattern of this sample is contributed mainly by gypsum and quartz. Additional peaks are likely due to Na-jarosite. The VNIR spectra of sample RTNP10 are highly consistent with gypsum, matching the triplet at 1.44, 1.49, and 1.54  $\mu\text{m}$ , the bands near 1.75 and 1.94  $\mu\text{m}$ , and exhibiting the doublet at 2.20 and 2.26  $\mu\text{m}$ . Some ferrihydrite is likely present as well due to the broadening of the  $\text{Fe}^{3+}$  band near 0.9  $\mu\text{m}$  and the water bands near 1.4 and 1.9  $\mu\text{m}$ , and some goethite is consistent with these spectra due to the shoulder near 0.6  $\mu\text{m}$ .

The Raman spectrum of the RTNP10 sample is similar to the spectrum RTNP05b in the low- and mid-wavenumber regions. However, the RTNP10 Raman spectrum shows two sharp bands at 3405 and 3492  $\text{cm}^{-1}$  at approximately the same position as those in the RTNP05b spectrum. The relative intensities of these pair of bands are, however, inverted in the RTNP10 spectrum. This is likely due to different crystal orientation—see Iishi (1979) for a detailed explanation of this phenomenon. Gypsum is the only mineral phase identified from the Raman spectrum of sample RTNP10.

## IMPLICATIONS

Table 1 summarizes the results from the three techniques used for the analysis of the Rio Tinto sulfates. A range of mineral phases were detected within the samples, including jarosite, Na-jarosite, gypsum, goethite, copiapite, ferricopiapite, and ferrihydrite. The XRD technique detected quartz in some of the samples, however no traces of this component were detected by the other techniques. It is likely that the rock substrate underneath the sulfate layers contained quartz crystals. While VNIR reflectance and Raman, as non-destructive spectroscopic techniques, yielded information from the surface layers alone, the powder used for the XRD analyses contained both sulfate layer and rock substrate grains, and thus information from the latter is retrieved from the XRD patterns.

Raman detection of ferrihydrite and goethite is difficult when mixed with  $\text{Fe}^{2+}$  and  $\text{Fe}^{3+}$  sulfates because sulfate and Fe-O interaction bands overlap in the low-wavenumber region.

VNIR reflectance facilitated the identification of various sulfate compounds in each of the samples, while XRD and Raman only provided positive identification of one or two different

◀FIGURE 7. Raman spectra (red circles) of sample RTNP05 in three regions of interest, spectral bands (gray), and fitted spectrum (black). Spectra 05a and 05b are offset for clarity. Jarosite and gypsum were identified based on the position and relative intensity of the spectral bands. (Color online.)

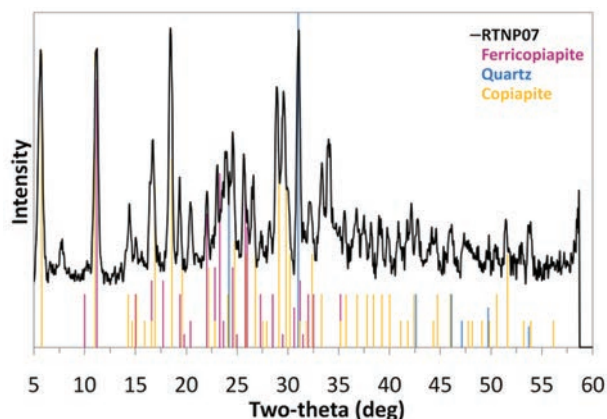


FIGURE 8. XRD pattern of sample RTNP07. The main peaks in the pattern match those of copiapite, jarosite, and quartz. (Color online.)

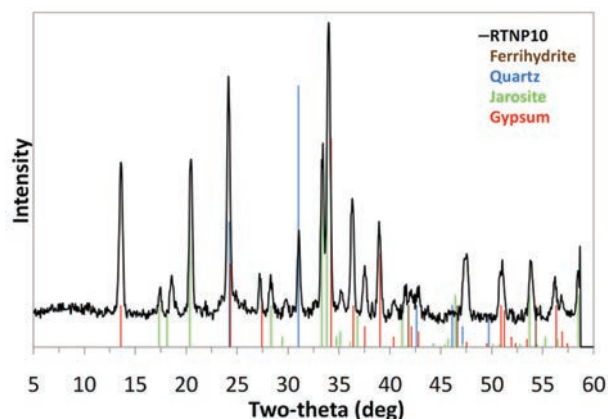


FIGURE 11. XRD pattern of sample RTNP010. The main peaks in the pattern match those of gypsum, quartz, and Na-jarosite. (Color online.)

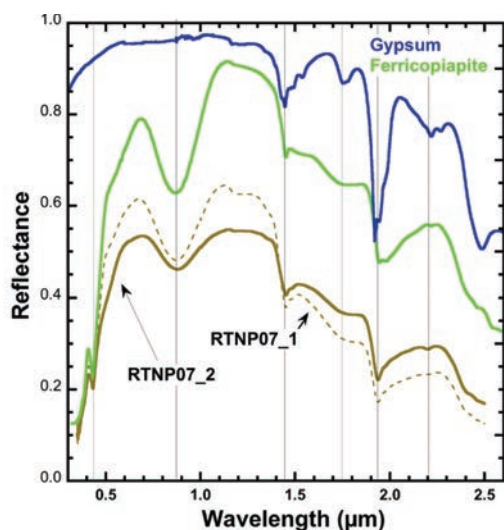


FIGURE 9. VNIR reflectance spectra of sample RTNP07. The spectra compare to those of gypsum (JB556) and ferricopiapite (JB620). (Color online.)

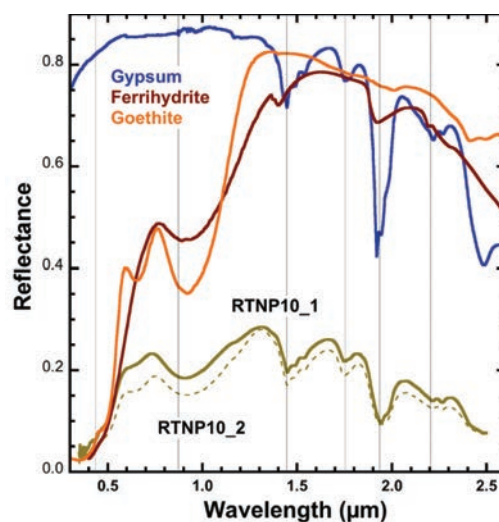


FIGURE 12. VNIR reflectance spectrum of sample RTNP010 and database spectra of gypsum (JB556), goethite (JB54), and ferrihydrite (JB499). (Color online.)

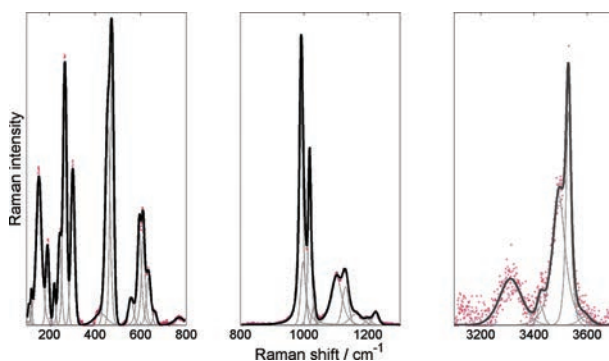


FIGURE 10. Raman spectrum (red circles) of sample RTNP07 in three regions of interest, spectral bands (gray), and fitted spectrum (black). Hydrated iron oxides were identified based on the position and relative intensity of the spectral bands. (Color online.)

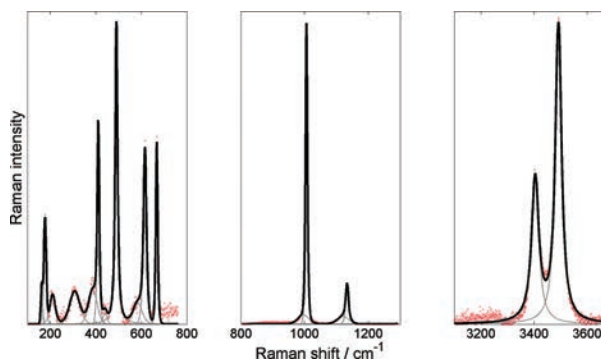


FIGURE 13. Raman spectrum (red circles) of sample RTNP010 in three regions of interest, spectral bands (gray), and fitted spectrum (black). Gypsum was identified based on the position and relative intensity of the spectral bands. (Color online.)

**TABLE 1.** Summary of the mineral identification

Sample ID	RTNP03	RTNP05	RTNP07	RTNP10
XRD	Gypsum, Quartz, Na-jarosite	Gypsum, K-jarosite	Copiapite, K-jarosite, Quartz	Gypsum, K-jarosite, Quartz
VNIR	K-jarosite, Gypsum, Goethite	K-jarosite, Gypsum, Goethite, Ferrihydrite, Ferricopiapite	Ferricopiapite, Gypsum	Gypsum, Ferrihydrite, Goethite
LRS	K-jarosite, UnID sulfate	Gypsum, K-jarosite	Ferricopiapite	Gypsum

phases; the VNIR reflectance spectra were measured from spots ~1 cm across, notably increasing the probability of finding multiple components in a single spectrum. On the other hand, such a large spot size prevented the detection of microscopic inclusions in the mineral matrices.

VNIR reflectance is uniquely suited for the characterization of water units and anions in minerals; however, water is a very intense absorber and may mask the reflectance of the cation-hydroxyl units (M-OH, where M represents a metallic cation). For this reason, the identification of spectral features associated with hydrated minerals in the VNIR spectra is not always unambiguous. One of the advantages of Raman is that water is a relatively poor scatterer, and hence the hydroxyl stretching of the M-OH units can be better resolved. As a result, more accurate band assignments can be achieved.

One of the difficulties associated with iron- and sulfate-bearing compounds collected in fieldwork is that they are often found to be poorly crystalline, making detection using XRD and Raman spectroscopy difficult. In these instances, VNIR reflectance frequently enables better detection of sulfate materials.

The small differences observed upon interpretation of the results from XRD, VNIR reflectance, and Raman spectroscopy of four natural samples from the Rio Tinto Mars analog provide a complete picture of the mineralogical composition of the samples, thus demonstrating that the three techniques are fully complementary and could be used simultaneously for the characterization of sulfate- and iron-rich mineralogy without sample preparation (except for XRD) and down to the crystal size (Raman).

In highly hydrated samples, Raman and XRD complement VNIR reflectance by unambiguously identifying different phases. For poorly crystalline samples, VNIR reflectance provides a more robust mineral identification, overcoming the difficulties associated with XRD and Raman spectroscopy.

In summary: the combined use of the Raman, VNIR reflectance, and XRD techniques is widely justified for achieving unique mineral identification of Fe-bearing oxides and sulfates on natural samples from acidic Mars analog sites, and likely on samples from Mars surface and surface. Synergies between these three techniques should be explored in the context of the science objectives of future Mars missions, e.g., ESA's ExoMars and NASA's Mars 2020 through assessing their potential to characterize other types of minerals relevant to Mars exploration.

## ACKNOWLEDGMENTS

This work was partially supported by the Research Council of Spain (CSIC) through grant no. UAC2005-007 and the NASA Astrobiology Institute through the Lewis and Clark Fund for Exploration and Field Research in Astrobiology. The authors thank Aurelio Sanz and Tayro Acosta for their valuable assistance in the collection and preservation of samples.

## REFERENCES CITED

- Amils, R., González-Toril, E., Fernández-Remolar, D., Gómez, F., Rodríguez, N., and Durán, C. (2002) Interaction of the sulfur and iron cycles in the Tinto River ecosystem. *Reviews in Environmental Science and Biotechnology*, 1, 299–309.
- Amils, R., Gonzalez-Toril, E., Fernandez-Remolar, D., Gomez, F., Aguilera, A.,

- Rodriguez, N., Malki, M., Garcia-Moyano, A., Fairen, A.G., de la Fuente, V., and Sanz, J.L. (2007) Extreme environments as mars terrestrial analogs: The Rio Tinto case. *Planetary and Space Science*, 55, 370–381.
- Bibring, J.-P., Arvidson, R.E., Gendrin, A., Gondet, B., Langevin, Y., Le Mouélic, S., Mangold, N., Morris, R.V., Mustard, J.F., Poulet, F., Quantin, C., and Sotin, C. (2007) Coupled ferric oxides and sulfates on the martian surface. *Science*, 317, 1206–1210.
- Bishop, J.L., and Murad, E. (2002) Spectroscopic and geochemical analyses of ferrihydrite from springs in Iceland and applications to Mars. *Geological Society, London, Special Publications*, 202, 357–370.
- (2005) The visible and infrared spectral properties of jarosite and alunite. *American Mineralogist*, 90, 1100–1107.
- Bishop, J.L., Murad, E., Lane, M.D., and Mancinelli, R.L. (2004) Multiple techniques for mineral identification on Mars: A study of hydrothermal rocks as potential analogues for astrobiology sites on Mars. *Icarus*, 169(2), 311–323.
- Bishop, J.L., Dyar, M.D., Lane, M.D., and Banfield, J.F. (2005) Spectral identification of hydrated sulfates on Mars and comparison with acidic environments on Earth. *International Journal of Astrobiology*, 3, 275–285.
- Bishop, J.L., Parente, M., Weitz, C.M., Noe Dobrea, E.Z., Roach, L.A., Murchie, S.L., McGuire, P.C., McKeown, N.K., Rossi, C.M., Brown, and others. (2009) Mineralogy of Juventae Chasma: Sulfates in the light-toned mounds, mafic minerals in the bedrock, and hydrated silica and hydroxylated ferric sulfate on the plateau. *Journal of Geophysical Research*, 114, E00D09, doi: 10.1029/2009JE003352.
- Blake, D., Vaniman, D., Achilles, C., Anderson, R., Bish, D., Bristow, T., Chen, C., Chipera, S., Crisp, J., Des Marais, D., and others. (2012) Characterization and calibration of the CheMin mineralogical instrument on Mars Science Laboratory. *Space Science Reviews*, 170, 341–399.
- Boston, P.J., Spilde, M.N., Northup, D.E., Melim, L.A., Soroka, D.S., Kleina, L.G., Lavoie, K.H., Hose, L.D., Mallory, L.M., Dahm, C.N., Crossey, L.J., and Schellble, R.T. (2001) Cave biosignature suites: Microbes, minerals, and Mars. *Astrobiology*, 1, 25–55.
- Chio, C.H., Sharma, S.K., and Muenow, D.W. (2005) Micro-Raman studies of hydrous ferrous sulfates and jarosites. *Spectrochimica Acta Part A-Molecular and Biomolecular Spectroscopy*, 61, 2428–2433.
- Christensen, P.R., Bandfield, J.L., Clark, R.N., Edgett, K.S., Hamilton, V.E., Hoefen, T., Kieffer, H.H., Kuzmin, R.O., Lane, M.D., Malin, M.C., and others. (2000) Detection of crystalline hematite mineralization on Mars by the Thermal Emission Spectrometer: Evidence for near-surface water. *Journal of Geophysical Research*, 105, 9623–9642.
- Christensen, P.R., Morris, R.V., Lane, M.D., Bandfield, J.L., and Malin, M.C. (2001) Global mapping of Martian hematite mineral deposits: Remnants of water-driven processes on early Mars. *Journal of Geophysical Research*, 106, 23873–23885.
- Clegg, S.M., Mangold, N., Le Mouélic, S., Olilla, A., Anderson, R., Blaney, D.L., Clark, B., Cousin, A., Dyar, M.D., Ehlmann, B.L., and others. (2013) High calcium phase observations at Rocknest with ChemCam. 44th Lunar and Planetary Science Conference, LPI Contribution 1719, p. 2087.
- Farrand, W.H., Glotch, T.D., Rice, J.W. Jr., Hurowitz, J.A., and Swayze, G.A. (2009) Discovery of jarosite within the Mawrth Vallis region of Mars: Implications for the geologic history of the region. *Icarus*, 204, 478–488.
- Fernández-Remolar, D.C., Morris, R.V., Gruener, J.E., Amils, R., and Knoll, A.H. (2005) The Rio Tinto basin, Spain: Mineralogy, sedimentary geobiology, and implications for interpretation of outcrop rocks at Meridiani Planum, Mars. *Earth and Planetary Science Letters*, 240, 149–167.
- Fernández-Remolar, D.C., Prieto-Ballesteros, O., Gómez-Ortiz, D., Fernández-Sampedro, M., Sarrazin, P., Gailhanou, M., and Amils, R. (2011) Rio Tinto sedimentary mineral assemblages: A terrestrial perspective that suggests some formation pathways of phyllosilicates on Mars. *Icarus*, 211, 114–138.
- Flahaut, J., Quantin, C., Allemand, P., Thomas, P., and Le Deit, L. (2010) Identification, distribution and possible origins of sulfates in Capri Chasma (Mars), inferred from CRISM data. *Journal of Geophysical Research: Planets*, 115, E11007, doi: 10.1029/2009JE003566.
- Frost, R.L., Wills, R.A., Weier, M.L., and Martens, W. (2005) Comparison of the Raman spectra of natural and synthetic K- and Na-jarosites at 298 and 77 K. *Journal of Raman Spectroscopy*, 36, 435–444.
- Frost, R.L., Wills, R.A., Klopogge, J.T., and Martens, W. (2006) Thermal decomposition of ammonium jarosite (NH<sub>4</sub>)Fe<sub>3</sub>(SO<sub>4</sub>)<sub>2</sub>(OH)<sub>6</sub>. *Journal of Thermal Analysis and Calorimetry*, 84, 489–496.
- Gellert, R., Rieder, R., Bruckner, J., Clark, B.C., Dreibus, G., Klingelhofer, G., Lugmair, G., Ming, D.W., Wanke, H., Yen, A., Zipfel, J., and Squires, S.W. (2006) Alpha particle X-ray spectrometer (APXS): Results from Gusev crater



- and calibration report. *Journal of Geophysical Research-Planets*, 111, E02S05.
- Gendrin, A., Mangold, N., Bibring, J.P., Langevin, Y., Gondet, B., Poulet, F., Bonello, G., Quantin, C., Mustard, J., Arvidson, R., and LeMouélic, S. (2005) Sulfates in martian layered terrains: The OMEGA/Mars Express view. *Science*, 307, 1587–1591.
- Haskin, L.A., Wang, A., Jolliff, B.L., McSween, H.Y., Clark, B.C., Des Marais, D.J., McLennan, S.M., Tosca, N.J., Hurowitz, J.A., Farmer, J.D., and others. (2005) Water alteration of rocks and soils on Mars at the Spirit rover site in Gusev crater. *Nature*, 436, 66–69.
- Hester, R.E., and Plane, R.A. (1964) Solvation of metal ions in aqueous solutions: the metal-oxygen bond. *Inorganic Chemistry*, 3, 768–769.
- Iishi, K. (1979) Phononspectroscopy and lattice dynamical calculations of anhydrite and gypsum. *Physics and Chemistry of Minerals*, 4, 341–359.
- Johnson, J.R., Bell, J.F., Cloutis, E., Staid, M., Farrand, W.H., McCoy, T., Rice, M., Wang, A., and Yen, A. (2007) Mineralogic constraints on sulfur-rich soils from Pancam spectra at Gusev crater, Mars. *Geophysical Research Letters*, 34, L13202.
- Klingelhofer, G., Morris, R.V., Bernhardt, B., Schroder, C., Rodionov, D.S., de Souza, P.A., Yen, A., Gellert, R., Evlanov, E.N., Zubkov, B., and others. (2004) Jarosite and hematite at Meridiani Planum from Opportunity's Mossbauer spectrometer. *Science*, 306, 1740–1745.
- Krishnamurthy, N., and Soots, V. (1971) Raman spectrum of gypsum. *Canadian Journal of Physics*, 49, 885–896.
- Lane, M.D., Bishop, J.L., Dyar, M.D., King, P.L., Parente, M., and Hyde, B.C. (2008) Mineralogy of the Paso Robles soils on Mars. *American Mineralogist*, 93, 728–739.
- Lichtenberg, K.A., Arvidson, R.E., Morris, R.V., Murchie, S.L., Bishop, J.L., Remolar, D.F., Glotch, T.D., Dobre, E.N., Mustard, J.F., Andrews-Hanna, J., and Roach, L.H. (2010) Stratigraphy of hydrated sulfates in the sedimentary deposits of Aram Chaos, Mars. *Journal of Geophysical Research-Planets*, 115, E00D17.
- Marquardt, D.W. (1963) An algorithm for least-squares estimation of non-linear parameters. *Journal of the Society for Industrial and Applied Mathematics*, 11, 431–441.
- Meslin, P.-Y., Gasnault, O., Forni, O., Schröder, S., Cousin, A., Berger, G., Clegg, S.M., Lasue, J., Maurice, S., Sautter, V., and others. (2013) Soil diversity and hydration as observed by ChemCam at Gale Crater, Mars. *Science*, 341, 6153, doi: 10.1126/science.1238670.
- Ming, D.W., Gellert, R., Morris, R.V., Arvidson, R.E., Brückner, J., Clark, B.C., Cohen, B.A., d'Uston, C., Economou, T., Fleischer, I., and others. (2008) Geochemical properties of rocks and soils in Gusev Crater, Mars: Results of the alpha particle X-ray spectrometer from Cumberland Ridge to Home Plate. *Journal of Geophysical Research*, 113, E12S39.
- Murchie, S.L., Mustard, J.F., Ehlmann, B.L., Milliken, R.E., Bishop, J.L., McKewin, N.K., Noe Dobre, E.Z., Seelos, F.P., Buczowski, D.L., Wiseman, S.M., and others. (2009) A synthesis of Martian aqueous mineralogy after 1 Mars year of observations from the Mars Reconnaissance Orbiter. *Journal of Geophysical Research*, 114, E00D06, doi: 10.1029/2009JE003342.
- Nakamoto, K. (1997) *Infrared and Raman Spectra of Inorganic and Coordination Compounds: Applications in coordination, organometallic, and bioinorganic chemistry*. Wiley, New York.
- Parente, M., Bishop, J.L., and Bell, J.F. (2009) Spectral unmixing for mineral identification in Pancam images of soils in Gusev Crater, Mars. *Icarus*, 203, 421–436.
- Rietveld, H. (1969) A profile refinement method for nuclear and magnetic structures. *Journal of Applied Crystallography*, 2, 65–71.
- Roach, L.H., Mustard, J.F., Murchie, S.L., Bibring, J.-P., Forget, F., Lewis, K.W., Aharonson, O., Vincendon, M., and Bishop, J.L. (2009) Testing Evidence of recent hydration state change in sulfates on Mars. *Journal of Geophysical Research (CRISM special issue)*, 114, E00D02, doi: 10.1029/2008JE003245.
- Roach, L.H., Mustard, J.F., Lane, M.D., Bishop, J.L., and Murchie, S.L. (2010) Diagenetic haematite and sulfate assemblages in Valles Marineris. *Icarus*, 207, 659–674.
- Sarrazin, P., Brunner, W., Blake, D., Gailhanou, M., Bish, D.L., Vaniman, D.T., Chipera, S.J., Ming, D.W., Steele, A., Midkandal, I., Amundsen, H., and Peterson, R. (2008) Field studies of Mars analog materials using a portable XRD/XRF instrument. 39th Lunar and Planetary Science Conference, (Lunar and Planetary Science XXXIX), LPI Contribution 1391, p. 2421.
- Sasaki, K., Tanaike, O., and Konno, H. (1998) Distinction of jarosite-group compounds by Raman spectroscopy. *Canadian Mineralogist*, 36, 1225–1235.
- Smith, P.H., Tamppari, L.K., Arvidson, R.E., Bass, D., Blaney, D., Boynton, W.V., Carswell, A., Catling, D.C., Clark, B.C., Duck, T., and others. (2009) H<sub>2</sub>O at the Phoenix Landing Site. *Science*, 325, 58–61.
- Sobron, P., Rull, F., Sobron, F., Sanz, A., Medina, J., and Nielsen, C.J. (2007) Modeling the physico-chemistry of acid sulfate waters through Raman spectroscopy of the system FeSO<sub>4</sub>-H<sub>2</sub>SO<sub>4</sub>-H<sub>2</sub>O. *Journal of Raman Spectroscopy*, 38, 1127–1132.
- Sobron, P., Sobron, F., Sanz, A., and Rull, F. (2008) Raman signal processing software for automated identification of mineral phases and biosignatures on Mars. *Applied Spectroscopy*, 62, 364–370.
- Sobron, P., Sansano, A., and Sanz, A. (2011) Evaporation pathways and solubility of Fe-Ca-Mg-rich salts in acid sulfate waters. A model for Martian ancient surface waters. *American Geophysical Union, Fall Meeting 2011*, abstract P23B-1712.
- Sowe, M., Wendt, L., McGuire, P.C., and Neukum, G. (2012) Hydrated minerals in the deposits of Aureum Chaos. *Icarus*, 218, 406–419.
- Tokar, R.L., Wiens, R.C., Maurice, S., Lasue, J., Johnson, J.R., Anderson, R.B., Cousin, A., Forni, O., Delapp, D.M., Lanza, N.L., and others. (2013) Searching for Chemical Variation Across the Surface of RockNest\_3 Using MSL ChemCam Spectra. LPI Contribution 1719, 1283.
- Wang, A., Haskin, L.A., Squyres, S.W., Jolliff, B.L., Crumpler, L., Gellert, R., Schröder, C., Herkenhoff, K., Hurowitz, J., Tosca, N.J., and others. (2006) Sulfate deposition in subsurface regolith in Gusev crater, Mars. *Journal of Geophysical Research*, 111, E02S17.
- Wang, A., Bell, J.F., Rice, M.S., and Cloutis, E.A. (2008) Coexistence of Si-rich and S-rich materials at Gusev Crater, Columbia Hills. 39th Lunar and Planetary Science Conference (Lunar and Planetary Science XXXIX), LPI Contribution 1391, p. 2186.
- Weitz, C.M., Bishop, J.L., Thollot, P., Mangold, N., and Roach, L.H. (2011) Diverse mineralogies in two troughs of Noctis Labyrinthus, Mars. *Geology*, 39, 899–902, doi: 10.1130/G32045.1.
- Wiseman, S.J., Arvidson, R.E., Morris, R.V., Poulet, F., Andrews-Hanna, J.C., Bishop, J.L., Murchie, S.L., Seelos, F.P., Des Marais, D., and Griffes, J.L. (2010) Spectral and stratigraphic context of hydrated sulfate and phyllosilicate deposits in Northern Sinus Meridiani, Mars. *Journal of Geophysical Research (CRISM special issue)*, 115, E00D18, doi: 10.1029/2009JE003354.

MANUSCRIPT RECEIVED MAY 10, 2013

MANUSCRIPT ACCEPTED JANUARY 21, 2014

MANUSCRIPT HANDLED BY MELISSA LANE